Vibration Analysis of Piezoelectric Materials by Optical Methods

Hsien-Yang Lin, Jin H. Huang, and Chien-Ching Ma

Abstract—**This study provides two noncontact and real-time optical measurement methods to assess the displacement, natural frequencies, and mode shapes of a vibrating piezoelectric material. The methods are carried out using amplitude-fluctuation electronic speckle pattern interferometry (AF-ESPI) and laser Doppler vibrometer (LDV), which are full-field and point-wise displacement measurement, respectively. Because the fringe patterns measured by AF-ESPI appear as a clear picture at the natural frequency, both natural frequencies and mode shapes of the vibrating material can be successfully obtained. In the LDV system, a swept-sine excitation signal from the function generator to the beam can result in a corresponding peak in frequency response curve at natural frequencies. From the frequency response curve, the natural frequencies are thus acquired. Measured results by both methods are seen to be in good agreement with theoretical predictions by the Galerkin method and finite element method.**

I. Introduction

PIEZOELECTRIC materials are typically used to generate an acoustic pulse from an input external loading (or electrical signal) and detect an acoustic pulse, then, convert it into a low impedance voltage signal. Research and development activities in these materials are now intense and widespread. Practical applications are numerous and spread across many areas such as sensors for active vibration control or actuators for precise motion control. This trend may account for why these materials constitute an important branch of the recently emerging technologies of modern engineering materials. A prominent feature of utilizing piezoelectric materials is the study of the full-field and real-time vibration behavior for piezoelectric materials. Therefore, so the reliable response of piezoelectric materials can be obtained, it is necessary to visibly examine the vibration response from an experimental point of view so the characteristics of the materials can be elucidated thoroughly. Thus, the present paper is aimed at filling this information need in this area and presents two noncontact and real-time optical methods for measurement of the vibration properties of piezoelectric materials.

Manuscript received March 20, 2001; accepted February 12, 2002. The authors would like to thank the National Science Council of the Republic of China for financially supporting this research under contracts No. NSC 89-2218-E-002-034 (CCM) and Nos. NSC 89-2212-E-035-003 and NSC 89-2745-P-035-004 (JHH).

H.-Y. Lin and C.-C. Ma are with the Department of Mechanical Engineering, National Taiwan University, Taipei, Taiwan 10617, Republic of China (e-mail: cma@w3.me.ntu.edu.tw).

J. H. Huang is with the Department of Mechanical Engineering, Feng Chia University, Taichung, Taiwan 40745, Republic of China.

The first optical measurement method is the electronic speckle pattern interferometry (ESPI) that is known as TV-holography or electro-optical holography. The ESPI combines the object and reference beams and directs them collinearly toward the detector array of frame-transfer charge-coupled device (CCD), which interfaces to a computer for video electronics processing of speckle patterns, then displays on a television-monitor in real time (about 30 ms). As compared with conventional holographic interferometry, the interferometric fringe patterns of ESPI are recorded using a video camera, thus eliminating the chemical film development process. Because the interferometric image is recorded and updated every 1/30 s, ESPI is faster and more insensitive to environment than holography. For these reasons, ESPI has become a powerful technique used in many academic researches and engineering applications. Due to ESPI using a video recording and display, its real-time nature makes it practical for vibration measurement. The first recorded work on ESPI is by Butters and Leendertz [1], who investigated the out-of-plane displacement of a vibrating disk. Since then, many researches have been forwarded in the area of deformation analysis [2], [3], especially for vibration measurement [4]–[6]. In an effort to increase image contrast, Ma and Huang [7], [8] further developed the amplitude-fluctuation ESPI (AF-ESPI) based on the work in [6]. From their works, AF-ESPI clearly displays the interferometric fringe patterns with high quality for identification of natural frequencies and mode shapes; therefore, this method will be adopted in this study.

The second optical measurement technique used in this work is the laser Doppler vibrometer (LDV), which measures the moving velocity or displacement of an object by detecting the frequency shift of the laser. This method has been used to meet various metrology needs for many years [9]–[11] because it provides precise noncontact measurement of particle motion on the solid surface and has an extremely wide signal bandwidth ranging from DC to 20 MHz and an ultra-high resolution better than nanometers. It appears that such a measurement system enables the dynamic study of piezoelectric materials.

Through these two optical measurement approaches, the displacements, natural frequencies, and mode shapes of a vibrating piezoelectric material with different boundary conditions are achieved. In addition, in light of the results presented in the work, theoretical predictions based on the Galerkin method and finite element method (FEM) utilizing ABAQUS commercial software package [12] also are made. The acceptable correspondence of the experimental data with numerical results reveals that the presented

methodologies on measuring vibration response of piezoelectric materials own an available exactitude.

II. Principle of Experimental Techniques

A. Amplitude Fluctuation Electronic Speckle Pattern Interferometry

The most familiar way of ESPI used for vibration analysis is the time-averaging method with an image sensor (mostly CCD array is used) integrating the speckle interferogram field pixel by pixel during camera frame period. Two different optical design setups are commonly used (out-of-plane sensitivity and in-plane sensitivity) for the vibration measurement. Fundamentals with regards to the AF-ESPI method for in-plane and out-of-plane measurement can be found in [7] and [8]. Because the piezoelectric material adopted in this work is thin, it will display larger transverse (out-of-plane) motion compared to any possible in-plane components, especially in the low natural frequencies. Hence, only the out-of-plane sensitivity optical setup is used in this study. As shown in Fig. 1, a He-Ne Laser (Uniphase 1135P, JDS Uniphase, San Jose, CA) with 30 mw and wavelength $\lambda = 632.8$ nm is used as the coherent light source. The emitting laser beam is split into two parts by a variable beamsplitter. One beam is directed toward the tested piezoelectric specimen, then reflects to the CCD camera acting as the object beam. The second one serves as a reference beam, is illuminated on the surface of a reference plate and reflects into the CCD camera via the beamsplitter. The object and reference beams are combined into the CCD sensor array through a zoom lens (Nikon Micro-Nikkor, 55 mm, Nikon, Melville, NY, USA). It is important to note that the optical path and the light intensity of these two beams should remain identical in the experimental setup. A CCD camera (Pulnix TM-7CN, Pulnix America, Inc., Sunnyvale, CA, USA) and a frame grabber (Dipix P360F, Dipix Technologies Inc., Ottawa, Ontario, Canada) with a digital signal processor on board are used to record and process the images obtained from interferogram of the object and reference beams. After the object is vibrating, the interferogram recorded by the CCD camera is stored in an image buffer as a reference image. The next frame then is grabbed and is subtracted by the image processing system. The CCD camera converts the intensity distribution of the interference pattern of the object into a corresponding video signal at 30 frames per second. The signal is electronically processed and converted into an image on the video monitor. The interpretation of the fringe image is similar to reading of a displacement contour. To achieve a sinusoidal output, a function generator (HP-33120A, Hewlett Packard, Palo Alto, CA) connected to a power amplifier (NF Electronic Instruments 4005 type, NF Corporation, Kohoku-ku, Yokohama, Japan) is used as an input source, which generates periodical exciting force to the specimen.

The detailed experimental procedure of the AF-ESPI technique is performed as follows. First, a reference image is taken after the specimen vibrates, then the second image is taken, and the reference image is subtracted by the image processing system. If the vibrating frequency is not at the natural frequency, only randomly distributed speckles are displayed and no fringe patterns will be shown. However, if the vibrating frequency is in the neighborhood of the natural frequency, stationary distinct fringe patterns will be observed. Then the function generator is cautiously and gradually turned, the number of fringes will increase and the fringe pattern becomes more clear; but, the position of nodal lines will not change as the natural frequency is approached. From the aforementioned experimental procedure, the natural frequencies and the corresponding mode shapes can be determined at the same time using the AF-ESPI optical system.

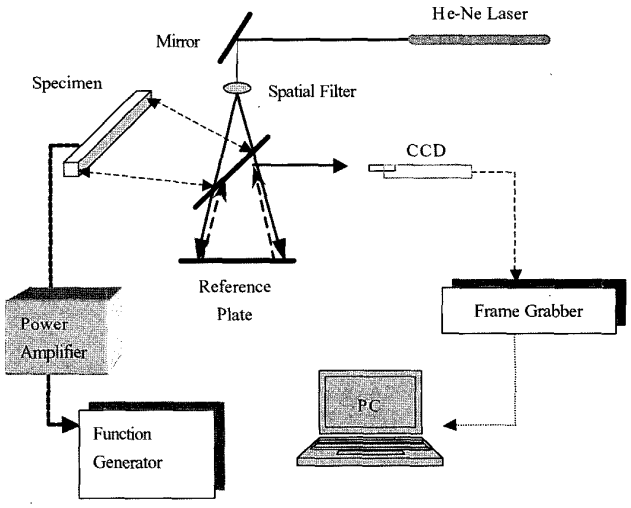

Fig. 1. Optical setup with out-of-plane sensitivity for ESPI.

B. Laser Doppler Vibrometer

The second optical technique used for measuring the dynamic response of piezoelectric materials is a LDV measurement system incorporated with the advanced vibrometer/interferometer device (AVID, AHEAD Optoelectronics, Inc., Chung-Ho, Taipei, Taiwan). A description of AVID's components and working principle is given in complete detail in [9], and is briefly outlined below. Instead of using an acoustic optical modulator, the AVID system utilizes circular polarization interference configuration, which can significantly reduce the size of the vibrometer and avoid the radio frequency (RF) electromagnetic interference effects created by the high frequency signal required to drive the acoustic optical modulator. With the circular polarization interference technique and digital signal processing with built-in phase decoding algorithms, the system can be designed to measure dynamic displacement and vibration responses of almost any object. The optical system, depicted in Fig. 2, for measuring dynamic displacements is based on the principle of the Michelson interferometer and the Doppler effect. In Fig. 2, a stabilized He-Ne laser is split into two interfered arms by

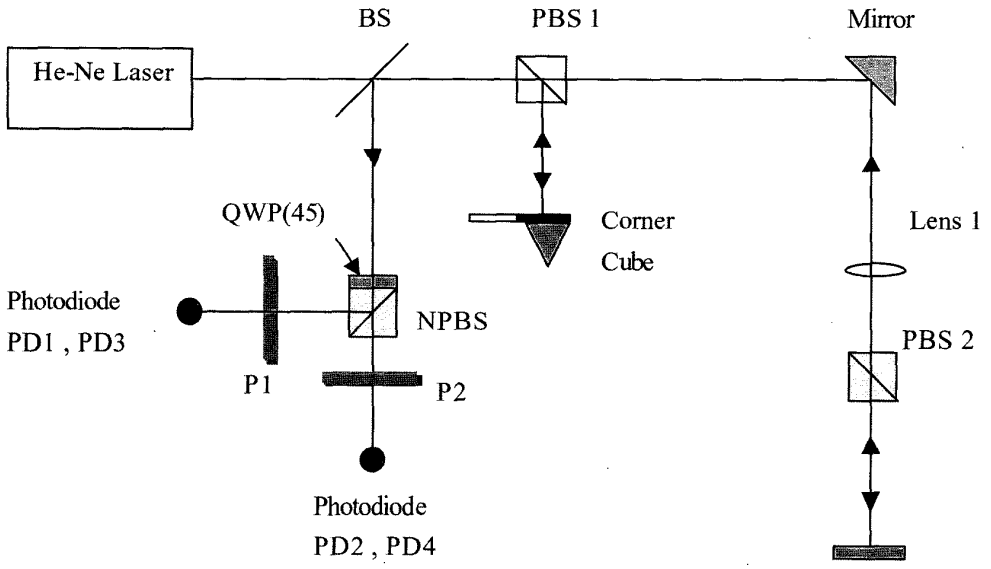

Fig. 2. Schematic diagram of the LDV optical setup for absolute displacement measurement [9].

the polarization beamsplitter (PBS1) within the optical head. Beam 1 passes through beamsplitter (PBS2) and is focused to a point on the tested object. For absolute displacement measurement, a corner cube reflects beam 2 acting as a reference beam. As beam 1 and beam 2 are split by PBS1, the two beams will possess "p" and "s" polarization states, respectively. These two returning beams after passing through PBS1 are linearly polarized and are orthogonal with each other, then reflected by a beamsplitter (BS). A quarter waveplate oriented at 45 degrees, denoted QWP(45), is used to transform the two returning light beams into a right circularly polarized light and a left circularly polarized light. The sum vector of the two circular polarized light beams can be viewed as a linearly polarized light with its polarization axis located at specific angle. Because the movement or displacement of the tested object will result in the different propagation speeds of the left- and right-hand polarized light, the two combined beams remain behaving like a linearly polarized light, but with an inclined angle relative to the horizontal axis due to the movement of tested object. The resultant linearly polarized light beam then is divided into two interfered light beams by a nonpolarization beamsplitter NPBS. Two polarizers P1 and P2, situated at 45 degrees apart, transforming the polarization states into quadrature intensity signals that can be detected by photodiodes, are utilized to make a 90-degree phase difference of the light intensity measured at respective photodiode PD1 to PD4. The four quadrature signals detected by photodiodes can be expressed as [13]:

$$\begin{aligned} I_1 &\propto [1+\sin(2\pi f_d t+\theta_0)],\\ I_2 &\propto [1+\cos(2\pi f_d t+\theta_0)],\\ I_3 &\propto [1-\sin(2\pi f_d t+\theta_0)],\\ I_4 &\propto [1-\cos(2\pi f_d t+\theta_0)], \end{aligned} \tag{1}$$

where f_d is the Doppler phase shift due to the movement, and θ_0 represents the relative phase difference between beam 1 and beam 2.

The signals P and Q standing for $I_1 - I_3$ and standing for $I_2 - I_4$, respectively, are amplified and shaped by the circuit board. These two signals differ by 90 degree phase angle are put into an analog-to-digital converter. By plotting these two signals P and Q on a X-Y plane, a Lissajous graph is constructed. That is, a circular pattern is formed when the phase difference between the two beams change by 360 degrees (or the tested object displaces half wavelength). Decoding the angle for any specific point on this circle is known as the P/Q signal decoding. Hence, by measuring the phase variation θ, one readily obtains the displacement D by the formula [9], [13]:

$$D = \frac{\theta}{2\pi} \times \frac{\lambda}{2} = f_d t \times \frac{\lambda}{2}. \tag{2}$$

Fig. 3 exhibits the LDV experimental setup adopted in the present work to examine the vibration behavior of piezoelectric materials. First, a function generator (HP-33120A) sends a swept sine-exciting signal to the power amplifier, then the amplified signal is input to the piezoelectric specimen, and the outgoing laser light is directed to a specific point of the upper surface of the specimen. Finally, the measured data in the time domain are transformed into frequency domain. As a result, we can easily identify the natural frequencies of piezoelectric materials from the spectrum response curve.

III. Theoretical Model for Piezoelectric Beam

A. Euler-Lagrange Equations and Natural Boundary Conditions

In this section, a simple and analytical model is proposed to examine the vibration response of a piezoelec-

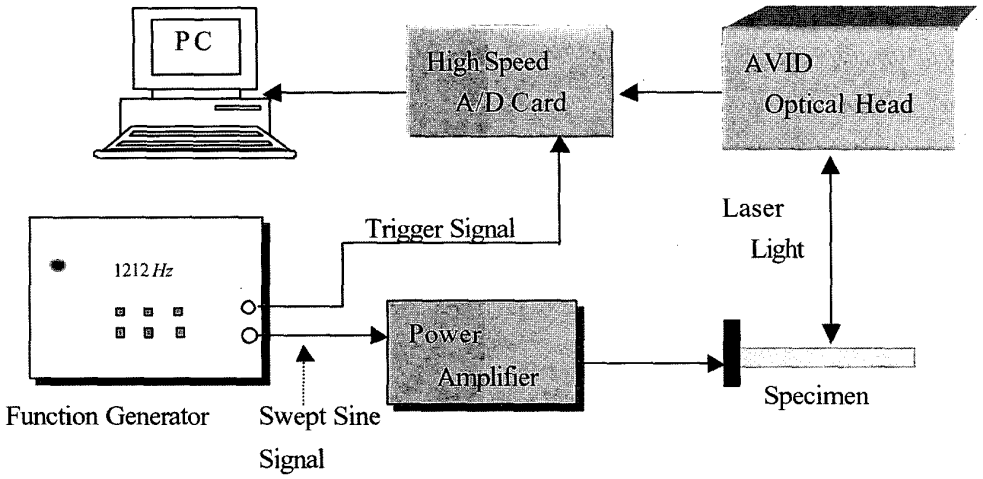

Fig. 3. Schematic diagram of the LDV measurement system for natural frequencies extraction.

tric material. Particular attention is devoted to a one-dimensional piezoelectric beam with arbitrary boundary conditions at the edges. More complicated two-dimensional model analysis can be found in [14], [15]. Now, consider a piezoelectric beam with electroded faces normal to thickness h or z direction as shown in Fig. 4. The linear piezoelectric constitutive equations coupled the electric and elastic fields for a 6 mm symmetry piezoelectric material are given by:

$$\begin{aligned} \sigma_{xx} &= C_{11}\varepsilon_{xx} - e_{31}E_z, \\ D_x &= e_{15}\varepsilon_{xz} + \kappa_{11}E_x, \\ D_z &= e_{31}\varepsilon_{xx} + \kappa_{33}E_z, \end{aligned} \tag{3}$$

where σ_{ij}, ε_{ij}, E_i, and D_i are stress, strain, electric field, and electric displacement, respectively; C_{ij}, e_{ij}, and κ_{ij} are elastic stiffness, piezoelectric coefficient, and dielectric constant, respectively. The strain and electric field components in (3) are in turn related to the deflection $w(x,t)$ and the electric potential $\phi(x,z,t)$ by the following relations:

$$\begin{aligned} \varepsilon_{xx} &= -zw_{,xx}, \\ E_x &= -\phi_{,x}, \\ E_y &= 0, \\ E_z &= -\phi_{,z}, \end{aligned} \tag{4}$$

in which the comma denotes the partial differentiation.

To derive the equations of motion for piezoelectric beams, adopt Hamilton's principle [14]:

$$\delta\Big\{\int \frac{1}{2}\left(\varepsilon_{ij}\sigma_{ij} - E_iD_i\right)dV - \int_{S_1}\left(\overline{p}w - \overline{\sigma}\phi\right)dS - \int_{S_2} n_iD_i\left(\phi - \overline{\phi}\right)dS\Big\} = 0, \tag{5}$$

where δ denotes the variational operator, V represents the volume of the beam, S_1 and S_2 stand for, respectively, the portion of the surface in which the transverse traction $\overline{p}$ and/or the electric charge $\overline{\sigma}$ are prescribed, and the portion of the surface on which the electrical potential $\overline{\phi}$ is prescribed, and n_i is the unit normal vector to S_2. Equation (5) allows us to derive the general equation governing electromechanical responses of a piezoelectric beam in the subsequent developments.

Suppose that the electric potential is expandable through the coordinate of beam thickness as:

$$\phi(x,z,t) = \phi^{(0)}(x,t) + z\phi^{(1)}(x,t) + z^2\phi^{(2)}(x,t), \tag{6}$$

where $\phi^{(0)}$, $\phi^{(1)}$, and $\phi^{(2)}$ are unknown electric potential parameters. Then, substituting (6) and (4) into (5), performing all of the integration, taking variations with respect to all variables, and collecting terms that contain variations of the same displacements and electric potentials, gives the governing equations:

$$\begin{aligned} C_{11}Iw_{,xxxx} - 2e_{31}I\phi^{(2)}_{,xx} + b\overline{p} &= \rho Aw_{,tt}, \\ 2e_{31}Iw_{,xx} - \kappa_{11}J\phi^{(2)}_{,xx} + 4\kappa_{33}I\phi^{(2)} - \kappa_{11}I\phi^{(0)}_{,xx} - b\overline{\sigma} &= 0, \\ \kappa_{11}I\phi^{(1)}_{,xx} - \kappa_{33}A\phi^{(1)} + b\overline{\sigma} &= 0, \\ \kappa_{11}I\phi^{(2)}_{,xx} + A\kappa_{11}\phi^{(0)}_{,xx} + b\overline{\sigma} &= 0, \end{aligned} \tag{7}$$

and the natural boundary conditions:

$$\begin{aligned} \left[C_{11}Iw_{,xxx} - 2e_{31}I\phi^{(2)}_{,x} + b\overline{p}\right]^L_0 &= 0, \\ \left[\kappa_{11}I\phi^{(0)}_{,x} + \kappa_{11}J\phi^{(2)}_{,x}\right]^L_0 &= 0, \\ \left[\kappa_{11}A\phi^{(0)}_{,x} + \kappa_{11}I\phi^{(2)}_{,x}\right]^L_0 &= 0, \\ -\kappa_{11}I\phi^{(1)}_{,x}\Big|^L_0 &= 0, \\ \phi - \overline{\phi}\Big|^h_0 &= 0, \end{aligned} \tag{8}$$

where $I = \dfrac{bh^3}{12}$, $J = \dfrac{bh^5}{80}$, and $A = bh$.

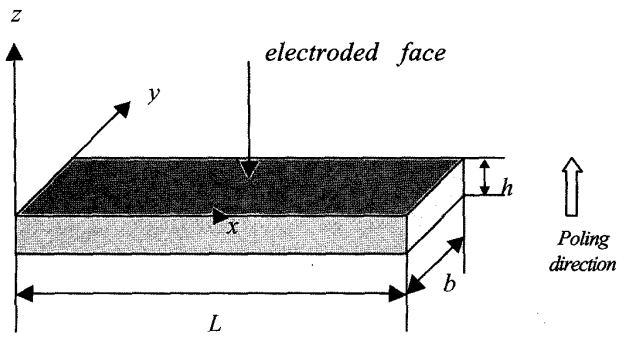

Fig. 4. Configuration of a piezoelectric beam.

It is observed from (6) and (7) that the electromechanical coupling due to the piezoelectric coefficient e_{31} vanishes when the electric potential is either a constant or a linear function of the beam thickness. This suggests that the electric potential is at least a quadratic function of the beam thickness. For this reason, we will examine the case of $\phi(x,z,t) = z^2\phi^{(2)}(x,t)$ only in the subsequent development.

Next, we adopt the Galerkin method [16] to obtain vibration response of the piezoelectric beam. When the same number of degrees of freedom is used, this method generally is much more effective than FEM. As illustrated examples, this methodology is described for clamped-free and clamped-clamped boundary conditions in order. According to the Galerkin method, the residual function $F_i(x,t)$ is required to be orthogonal to some weighting functions $\Gamma(x)$. That is:

$$\int_V F_i(x,t)\Gamma(x)dx = 0 \qquad (i=1,2,3), \tag{9}$$

where $\Gamma(x)$ may be chosen to be members of the approximate solution, and the residual functions can be obtained from the governing equations (7) as:

$$\begin{aligned} F_1(x,t) &= C_{11}Iw_{,xxxx} - 2e_{31}I\phi^{(2)}_{,xx} + \rho A\ddot{w}, \\ F_2(x,t) &= 2e_{31}Iw_{,xx} - \kappa_{11}J\phi^{(2)}_{,xx} + 4\kappa_{11}I\phi^{(2)} - \kappa_{11}I\phi^{(0)}_{,xx}, \\ F_3(x,t) &= \kappa_{11}I\phi^{(2)}_{,xx} + \kappa_{11}A\phi^{(0)}_{,xx}. \end{aligned} \tag{10}$$

The desired functions appearing in preceding equations are taken as:

$$\begin{aligned} w(x,t) &= \sum_{k=1}^{n} W_k\Gamma(x)e^{i\omega t}, \\ \phi^{(0)}(x,t) &= \sum_{k=1}^{n} \Phi_k^{(0)}\Gamma(x)e^{i\omega t}, \\ \phi^{(2)}(x,t) &= \sum_{k=1}^{n} \Phi_k^{(2)}\Gamma(x)e^{i\omega t}, \end{aligned} \tag{11}$$

in which W_k, $\Phi_k^{(0)}$, and $\Phi_k^{(2)}$ are unknown parameters, and ω is an excitation frequency.

B. Clamped-Free Boundary Condition

Parallel to the eigenfunction for elastic beam, the following weighting function satisfying the boundary conditions is assumed to be:

$$\begin{aligned} \Gamma(x) = &\left(\cos\frac{\lambda_i x}{L} - \cosh\frac{\lambda_i x}{L}\right) \\ &+ \frac{\sin\lambda_i - \cosh\lambda_i}{\cos\lambda_i + \cosh\lambda_i}\left(\sin\frac{\lambda_i x}{L} - \sinh\frac{\lambda_i x}{L}\right). \end{aligned} \tag{12}$$

Here the dimensionless natural frequency parameter, λ_i, can be numerically calculated from the equation:

$$\cos\lambda_i\cosh\lambda_i + 1 = 0. \tag{13}$$

Substituting (11)–(13) into (9) yields:

$$\left(\begin{bmatrix} a_{11} & a_{12} & 0 \\ -a_{12} & a_{22} & a_{23} \\ 0 & -a_{23} & a_{33} \end{bmatrix} - \omega^2 \begin{bmatrix} r_{11} & 0 & 0 \\ 0 & 0 & 0 \\ 0 & 0 & 0 \end{bmatrix}\right) \begin{Bmatrix} W_1 \\ \Phi_1^{(2)} \\ \Phi_1^{(0)} \end{Bmatrix} = 0, \tag{14}$$

where

$$\begin{aligned} a_{11} &= \pi^4 C_{11} I/2L^3, \\ a_{12} &= \pi^2 e_{31} I/L, \\ a_{22} &= 2\kappa_{33} IL + \pi^2\kappa_{11} J/2L, \\ a_{23} &= \frac{\pi^2\kappa_{11} I}{2}, \\ a_{33} &= \frac{-\pi^2\kappa_{11} A}{2L}, \\ r_{11} &= \rho LA/2. \end{aligned} \tag{15}$$

Thus, natural frequencies are readily obtained by solving the resulting eigenvalue problem as indicated in (14).

C. Clamped-Clamped Boundary Condition

Similarly, to satisfy the clamped-clamped boundary condition, the weighting function is taken as:

$$\begin{aligned} \Gamma(x) = &\left(\cos\frac{\lambda_i x}{L} - \cosh\frac{\lambda_i x}{L}\right) \\ &+ \frac{\sin\lambda_i + \sinh\lambda_i}{\cos\lambda_i - \cosh\lambda_i}\left(\sin\frac{\lambda_i x}{L} - \sinh\frac{\lambda_i x}{L}\right), \end{aligned} \tag{16}$$

in which λ_i satisfies:

$$\cos\lambda_i\cosh\lambda_i = 1. \tag{17}$$

Substituting (11), (16), and (13) into (9) gives:

$$\left(\begin{bmatrix} a_{11} & a_{12} & 0 \\ -a_{12} & a_{22} & a_{23} \\ 0 & -a_{23} & a_{33} \end{bmatrix} - \omega^2 \begin{bmatrix} r_{11} & 0 & 0 \\ 0 & 0 & 0 \\ 0 & 0 & 0 \end{bmatrix}\right) \begin{Bmatrix} W_1 \\ \Phi_1^{(2)} \\ \Phi_1^{(0)} \end{Bmatrix} = 0. \tag{18}$$

where

$$\begin{aligned} a_{11} &= 8\pi^4 C_{11} I/L^3, \\ a_{22} &= 6\kappa_{33} IL + 2\pi^2 \kappa_{11} J/L, \\ a_{33} &= -2\pi^2 \kappa_{11} A/L, \\ a_{12} &= 4\pi^2 e_{11} I/L, \\ a_{23} &= 2\pi^2 \kappa_{11} I/L, \\ r_{11} &= -3\rho AL/2. \end{aligned} \tag{19}$$

Following the same procedure outlined in the previous section, the natural frequencies can be obtained by (18).

In addition to the Galerkin method, numerical calculations of natural frequencies as well as mode shapes also are performed by the ABAQUS finite element commercial package, in which 20-node, three-dimensional, brick piezoelectric elements (C3D20RE, Hibbitt, Karlsson & Sorensen, Inc., Pawtucket, RI) are selected to analyze the problem. The total number of elements and nodes used are 102 and 1006, respectively. The numerical results obtained by Galerkin and FEM methods will be compared with those by the proposed optical methods in Section IV.

IV. Experimental and Numerical Results

The examples that will be illustrated in this section are clamped-free and clamped-clamped piezoelectric beams. The former is a $38 \times 2.5 \times 0.5$ mm piezoelectric cantilever beam made of Keramos K-270 (Keramos Advanced Piezoelectrics, Indianapolis, IN) piezoelectric ceramics. Its material properties are listed in Table I. To save space here, only the first five modes are presented. Fig. 5 summarizes the detailed modal parameters of the K-270 clamped-free piezoelectric beam. Those bold lines in FEM diagram appearing in the right-hand part of Fig. 5 are a symbol of nodal lines of the beam, which show good agreement with the nodal lines (the brightest lines) measured by AF-ESPI. In finite element results, dashed lines and "−" symbol denote the concave displacements; the solid lines and the "+" symbol stand for convex displacements.

In the AF-ESPI results, the fringes are contours of constant vibration amplitudes of the out-of-plane displacement. The related amplitude A_i can be quantitatively calculated by the roots R_i of the zero-order Bessel function of the first kind $\left|J_0(4\pi A_i \lambda)\right| = 0$, which represents the dark fringes in experimental measurement. The first 12 roots of R_i are 2.4, 5.52, 8.66, 11.79, 14.93, 18.07, 21.21, 24.35, 27.49, 30.63, 33.78, and 36.92. Then the corresponding amplitudes A_i of the out-of-plane displacement are evaluated by the following:

$$A_i = \frac{\lambda R_i}{4\pi}, \tag{20}$$

where $\lambda = 0.633$ μm.

The deflection curves of the first five vibration modes for the theoretical and experimental results are indicated in the left-hand part of Fig. 5. Excellent agreements are obtained. Table II tabulates the natural frequencies obtained from experimental and theoretical methods. The measured results of natural frequencies by the two optical methods agree well with theoretical predictions, but all are lower than those by the Galerkin method and FEM. This discrepancy is probably due to the thickness variation across the beam, the material properties measurement, and the clamped boundary condition of the specimen. It also is observed that the relative error of LDV compared with theoretical (Galerkin) values is larger than that of AF-ESPI in the interval of lower natural frequencies. This may be attributed to the scan rate (100 KHz) and sampling points (8192) of the LDV system. In other words, after transforming the time domain data, the interval of the data is 12.21 Hz (i.e., only 0, 12.21, 24.42, 36.63 ... Hz are displayed in a response curve). Such a large interval leads to a higher error ratio in the lower frequency region.

TABLE I
Material Properties of K-270 Piezoelectric Ceramics.

Quality	K-270
S_{11}^E (m^2/N)	12.1×10^{-12}
S_{12}^E	-4.03×10^{-12}
S_{13}^E	-5.3×10^{-12}
S_{33}^E	15.3×10^{-12}
S_{44}^E	38.9×10^{-12}
S_{66}^E	32.5×10^{-12}
d_{31} (Coul/Newton)	-120×10^{-12}
d_{33}	270×10^{-12}
d_{15}	490×10^{-12}
ρ (Kg/m^3)	7500
κ_{11} (F/m)	1.31×10^{-8}
κ_{33}	1.151×10^{-8}

Fig. 6 shows the frequency-response curve measured by the LDV system, in which the measured points are along the central line of the beam. The first five peaks corresponding to the first five natural frequencies are shown in good agreement with the measured values by AF-ESPI.

For the clamped-clamped piezoelectric beam, the specimen, dimensioned by $45 \times 2.5 \times 0.5$ mm, is also made of Keramos K-270 piezoelectric ceramics. Table III lists the first five natural frequencies determined by optical and numerical methods, respectively. Similar features are found for this case as compared with that in the clamped-free case. The discrepancies between the Galerkin and FEM results are less than 1%. Fig. 7 shows a frequency-response curve measured by the LDV system. The natural frequencies emerge clearly at the peak values in Fig. 7.

Fig. 8 shows the corresponding mode shapes and deflection curves for the first five natural frequencies. Excellent agreements are found for the experimental measurements and theoretical predictions. Moreover, owing to the actual beam specimens possessing the 2.5 mm width, hence not only the abovementioned bending modes but also the torsional modes may exist. Because the present AF-ESPI

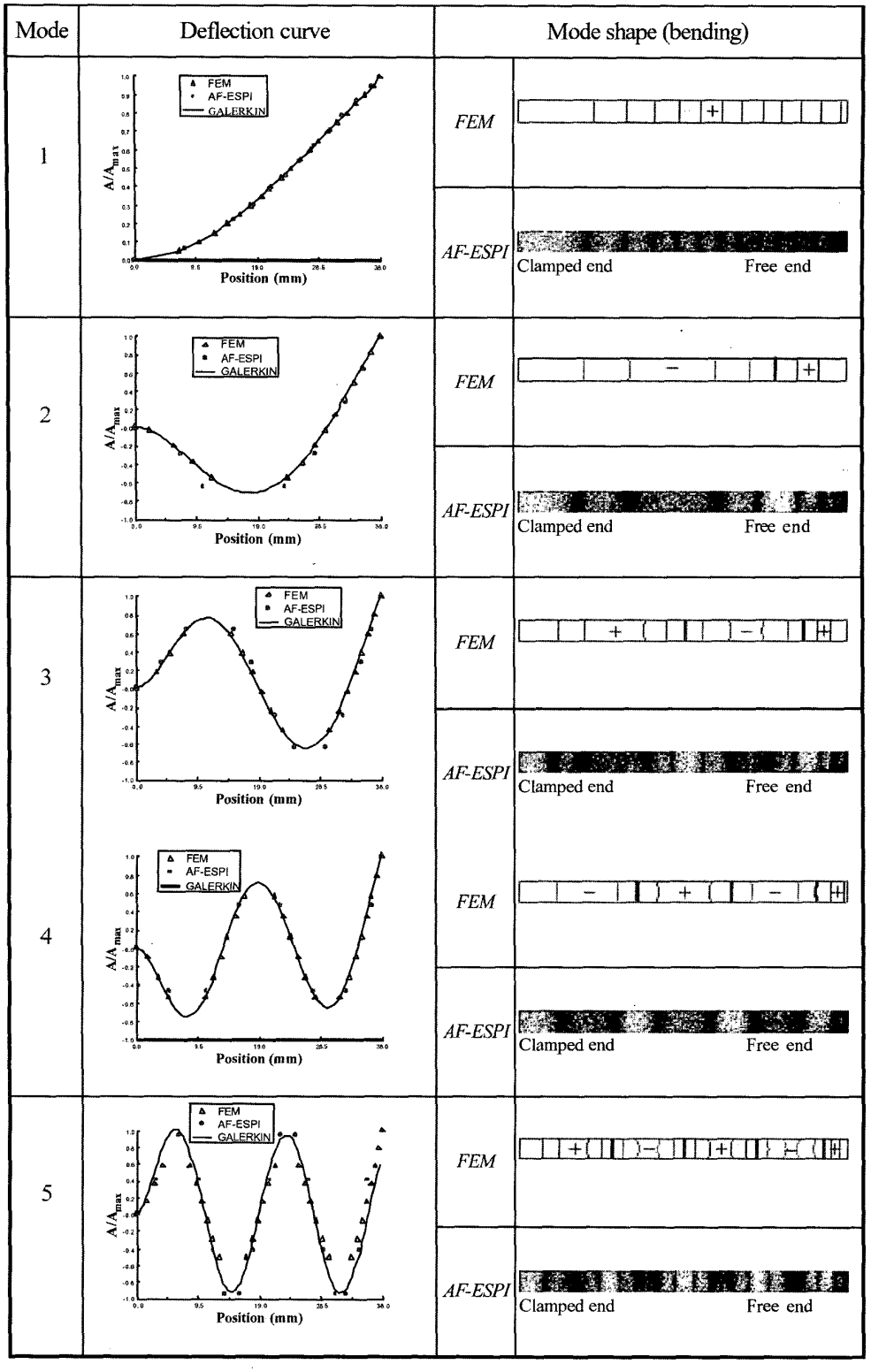

Fig. 5. Vibration properties of a K-270 clamped-free piezoelectric beam.

TABLE II

FIRST FIVE NATURAL FREQUENCIES BY OPTICAL AND THEORETICAL METHODS FOR A K-270 CLAMPED-FREE PIEZOELECTRIC BEAM (ERROR: COMPARED WITH THE GALERKIN METHOD).

Method	AF-ESPI		LDV		FEM	GALERKIN
	Natural frequency (Hz)	Error (%)	Natural frequency (Hz)	Error (%)	Natural frequency (Hz)	Natural frequency (Hz)
Mode 1	188	−5.05	171	−13.60	198	198
Mode 2	1190	−3.64	1111	−10.04	1232	1235
Mode 3	3254	−5.54	3210	−6.82	3448	3445
Mode 4	6298	−6.75	6396	−5.30	6754	6754
Mode 5	10420	−6.67	10682	−4.33	11160	11165

TABLE III

FIRST FIVE NATURAL FREQUENCIES BY OPTICAL AND THEORETICAL METHODS FOR A K-270 CLAMPED-CLAMPED PIEZOELECTRIC BEAM (ERROR: COMPARED WITH THE GALERKIN METHOD).

Method	AF-ESPI		LDV		FEM	GALERKIN
	Natural frequency (Hz)	Error (%)	Natural frequency (Hz)	Error (%)	Natural frequency (Hz)	Natural frequency (Hz)
Mode 1	856	−3.60	817	−8.00	897	888
Mode 2	2308	−6.10	2258	−8.14	2473	2458
Mode 3	4591	−4.67	4358	−9.51	4839	4816
Mode 4	7223	−9.28	7056	−11.38	7994	7962
Mode 5	11576	−2.67	10571	11.11	11934	11893

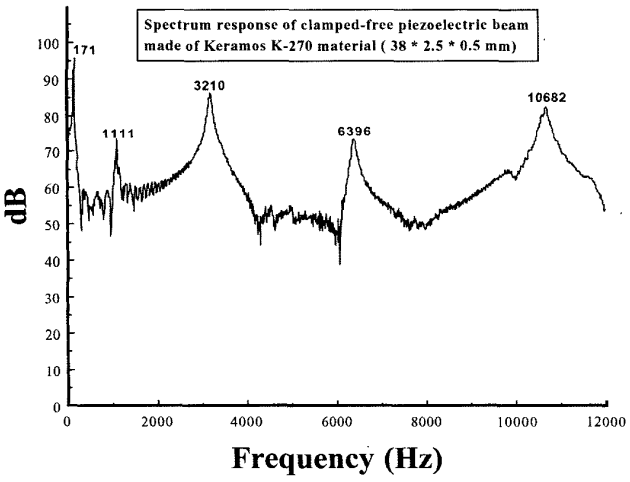

Fig. 6. Frequency response curve for a clamped-free piezoelectric beam measured by LDV.

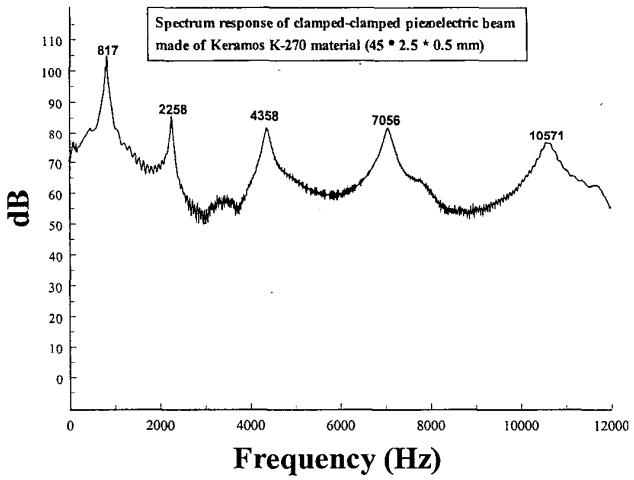

Fig. 7. Frequency response curve for a clamped-clamped piezoelectric beam measured by LDV.

optical system is a full-field measurement technique, the torsional modes also can be observed. Fig. 9 shows the torsional mode shapes observed by the AF-ESPI and calculated by FEM. Good agreement also is found for both approaches.

V. CONCLUSIONS

This work has examined the displacement, natural frequencies, and mode shapes of a vibrating piezoelectric material by using AF-ESPI and LDV. It has shown that the two optical methods have the advantages of noncontact, real-time, and high-resolution measurement for investigating the vibration problem of piezoelectric materials. Ac-

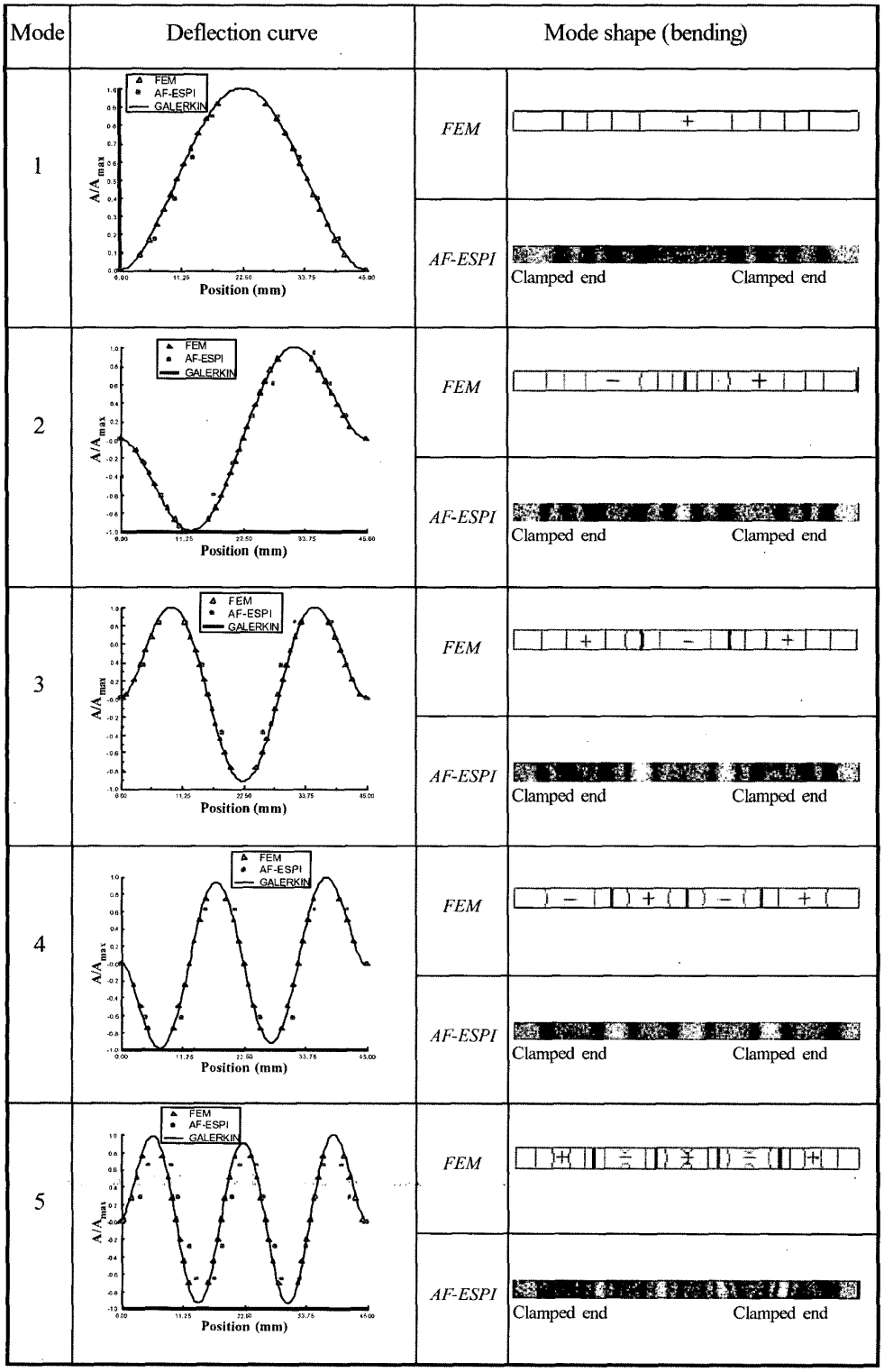

Fig. 8. Vibration properties of a K-270 clamped-clamped piezoelectric beam.

Boundary	Mode No	Method	Natural frequency(Hz)	Mode shape (torsion)
Clamped | Free	1	*FEM*	4957	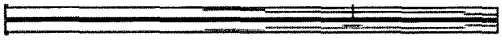
		AF-ESPI	4935	
	2	*FEM*	14908	
		AF-ESPI	14854	
Clamped | Clamped	1	*FEM*	8536	
		AF-ESPI	8456	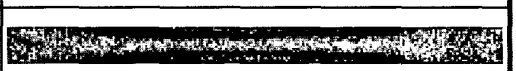
	2	*FEM*	17118	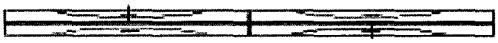
		AF-ESPI	17108	
	3	*FEM*	25797	
		AF-ESPI	23614	
	4	*FEM*	34616	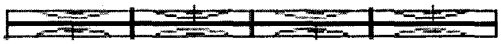
		AF-ESPI	30996	

Fig. 9. Torsional vibration mode parameters of K-270 piezoelectric beam by AF-ESPI and FEM.

cording to our results, the natural frequencies measured by AF-ESPI correlate well with LDV. The AF-ESPI enables both the full-field mode shapes and natural frequencies obtained at the same time. The LDV system obtains the natural frequencies rapidly and easily. The good correspondence of the experimental data with theoretical results by means of the Galerkin method and FEM verifies that the presented methodologies on measuring vibration response of piezoelectric materials have an available accuracy. These results also demonstrate that the optical techniques proposed herein are applicable to many situations in engineering vibration analysis for piezoelectric materials with different boundary conditions. Moreover, the proposed methodologies for measuring the out-of-plane vibration response of piezoelectric beams can be equally applied not only to measure in-plane response but also to gain simultaneously both out-of-plane and in-plane responses for any two-dimensional vibrating materials with/without piezoelectric coupling effect.

REFERENCES

[1] J. N. Butters and J. A. Leendertz, "Speckle patterns and holographic techniques in engineering metrology," *Opt. Laser Technol.*, vol. 3, no. 1, pp. 26–30, 1971.

[2] R. Jones and C. Wykes, *Holographic and Speckle Interferometry*. Cambridge, England: Cambridge Univ. Press, 1989.

[3] C. Wykes, "Use of electronic speckle pattern interferometry (ESPI) in the measurement of static and dynamic surface displacements," *Opt. Laser Technol.*, vol. 21, no. 3, pp. 400–406, 1982.

[4] K. Creath and A. Gudmunn, "Vibration-observation techniques for digital speckle-pattern interferometry," *J. Opt. Soc. Amer. A*, vol. 2, no. 10, pp. 1629–1636, 1985.

[5] S. Nakadate, "Vibration measurement using phase-shifting speckle pattern interferometry," *Appl. Opt.*, vol. 25, no. 22, pp. 4162–4167, 1986.

[6] W. C. Wang, C. H. Hwang, and S. Y. Lin, "Vibration measurement by the time-averaging electronic speckle pattern interferometry method," *Appl. Opt.*, vol. 35, no. 22, pp. 4502–4509, 1996.
[7] C. H. Huang and C. C. Ma, "Vibration characteristics for piezoelectric cylinders using amplitude-fluctuation electronic speckle pattern interferometry," *AIAA J.*, vol. 36, no. 12, pp. 2262–2268, 1998.
[8] C. C. Ma and C. H. Huang, "The investigation of three-dimensional vibration for piezoelectric rectangular parallelepipeds using the AF-ESPI method," *IEEE Trans. Ultrason., Ferroelect., Freq. Contr.*, vol. 48, no. 1, pp. 142–153, 2001.
[9] C. K. Lee and G. Y. Wu, "High performance Doppler interferometer for advanced optical storage system," *Jpn. J. Appl. Phys.*, vol. 38, no. 3B, pp. 1730–1741, 1999.
[10] B. K. A. Ngoi, K. Venkatakrishnan, and B. Tan, "Laser scanning heterodyne interferometer for micro-components," *Opt. Commun.*, vol. 173, pp. 291–301, 2000.
[11] O. Nishizawa, T. Satoh, and X. Lei, "Detection of shear wave in ultrasonic range by a laser Doppler vibrometer," *Rev. Sci. Instrum.*, vol. 69, no. 3, pp. 2572–2573, 1998.
[12] *ABAQUS User's Manual, version 5.8.* Pawtucket, RI: Hibbit, Karlsson, and Sorensen, Inc., pp. 23.16.7-1–23.16.7-2, 1998.
[13] *AVID User's Manual.* Chung-Ho, Taiwan: Ahead Optoelectronics, Inc., pp. 3-1–3-6.
[14] J. H. Huang and T. L. Wu, "Analysis of hybrid multilayered piezoelectric plates," *Int. J. Eng. Sci.*, vol. 34, no. 2, pp. 171–181, 1996.
[15] J. H. Huang and H. I. Yu, "Dynamic response of piezoelectric plates as sensors or actuators," *Mater. Lett.*, vol. 46, no. 11, pp. 70–80, 2000.
[16] T. Mura and T. Koya, *Variational Methods in Mechanics.* London: Oxford Univ. Press, 1992.

Hsien-Yang Lin received the B.S. degree in civil engineering from the Feng Chia University, Taiwan, the M.S. degree in mechanical engineering from the National Taiwan University, Taiwan, Republic of China, in 1984 and 1989, respectively. In 1990, he began working in Sez-Hai Institute of Technology and Commerence as a lecturer. Since 1998, he has been a graduate student in mechanical engineering at the National Taiwan University, Taiwan.

His research interests include the photomechanics and vibration analysis of piezoelectric materials.

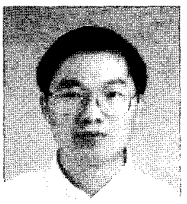

Jin H. Huang received the B.S. degree in mechanical engineering from the Feng Chia University, Taiwan, Republic of China, the M.S. degree in mechanical engineering from the University of New Mexico, Albuquerque, NM, and the Ph.D. degree in mechanical engineering from Northwestern University, Evanston, IL, in 1985, 1989, and 1992, respectively. Since 1993 he has been with the Feng Chia University, where he is currently a professor of mechanical engineering.

His research interests include the application of piezoelectric/piezomagnetic composites, magnetostriction of ferromagnetic composites, and effective material properties of composites.

Chien-Ching Ma received the B.S. degree in agriculture engineering from the National Taiwan University, Taiwan, in 1978 and the M.S. and Ph.D. degrees in mechanical engineering from Brown University, Providence, RI in 1982 and 1984, respectively. From 1984 to 1985, he worked as a postdoc in the Engineering Division, Brown University. In 1985, he joined the faculty of the Department of Mechanical Engineering, National Taiwan University, Taiwan, Republic of China, as an associate professor. He was promoted to full professor in 1989.

His research interests are in the fields of wave propagation in solids, fracture mechanics, solid mechanics, and vibration analysis.